Cytotherapy 27 (2025) 365–377

Contents lists available at ScienceDirect

CYTOTHERAPY

journal homepage: www.isct-cytotherapy.org

FULL-LENGTH ARTICLE

Exosome Therapy

Neural stem cell–derived extracellular vesicles purified by monolith chromatography retain stimulatory effect in *in vitro* scratch assay

Ivano Luigi Colao[1], Randolph L. Corteling[2], Daniel G. Bracewell[1,*], Ivan B. Wall[3,**]

[1] *Department of Biochemical Engineering, University College London, London, UK*
[2] *ReNeuron Ltd., Pencoed, UK*
[3] *Institute of Immunology and Immunotherapy, College of Medicine and Health, University of Birmingham, Birmingham, UK*

ARTICLE INFO

Article History:
Received 11 March 2024
Accepted 5 November 2024

Key Words:
extracellular vesicles
hydrophobic interaction
neural stem cells
quaternary amine
scratch assay
TFF

ABSTRACT

Background aims: Extracellular vesicles (EVs) have gained traction as potential cell-free therapeutic candidates. Development of purification methods that are scalable and robust is a major focus of EV research. Yet there is still little in the literature that evaluates purification methods against potency of the EV product. In the present study, we examined two monolith chromatography methods with a focus on assessing the ability of purified EVs to retain stimulatory effects on fibroblasts to connect scalable purification methods with product outputs.
Methods: We characterized EVs recovered from CTX0E03 (CTX) neural stem cell–conditioned medium in terms of biomarker distribution, functional capacity and purity. We evaluated the ability of EVs to promote wound closure in an *in vitro* scratch assay prior to and following two monolith chromatography steps (anion exchange and hydrophobic interaction) to determine whether these options may better serve EV bioprocessing.
Results: EVs from CTX cells were successful in initiating wound repair in a fibroblast scratch assay over 72 h with a single 20-μg dose. EV preparations presented the markers CD9, CD81 and CD63 but also contained culture albumin and DNA as process impurities. EVs recovered by tangential flow filtration could be successfully purified further by both monolith chromatography steps. Post-monolith EV stimulation was conserved.
Conclusions: The results indicate that monolith chromatography is a viable purification method for EVs derived from cell culture that does not detract from the product's ability to stimulate fibroblasts, suggesting that product functionality is conserved. Further work is needed in developing suitable downstream processes and analytics to achieve clinically relevant purities for injectable biologics.

Introduction

Extracellular vesicle (EV) research has experienced a surge in popularity. This is because EVs hold potential as native or bioengineered [1] therapeutic candidates [2,3] and can also be modified as targeted drug delivery vehicles [4–6]. To be translated into the clinic, research must tackle the challenges associated with scalable and clinically relevant preparation of EV products, which we have described previously in a perspective article highlighting the challenges and potential solutions for clinical EV manufacture [7], sentiments that have also been echoed by others [8–10].

To date, the scientific community has produced a wide range of articles on EVs as potential therapies and their functions [11–13] and, separately, on the methods used for their characterization and isolation [14–16]. Relatively little in the literature combines the outputs of how downstream processing (DSP) options relate to the final product potency, with an article from 2017 claiming to be the first to do this [17]. More recently, a 2023 article demonstrated how two variations of ultrafiltration kits yielded strikingly different variations in EV marker profiles and purity [18]. Although not directly related to potency, one might expect such variations to hinder EV studies (and the conclusions drawn).

Although some articles claim "large-scale" studies, the material is still often ≤1 L of conditioned medium [14]. Although large for current studies, this is insufficient for clinically relevant material volumes. This limitation in research is due to current challenges in cell therapy scaling [19,20]. The stem cell sources that constitute much of EV research (e.g., mesenchymal stromal cells) are often difficult and

* Correspondence: Daniel G. Bracewell, Department of Biochemical Engineering, University College London, Gower Street, London WC1E 6BT, UK.
** Correspondence: Ivan B. Wall, Institute of Immunology and Immunotherapy, College of Medicine and Health, University of Birmingham, Birmingham B15 2TT, UK.
E-mail addresses: d.bracewell@ucl.ac.uk (D.G. Bracewell), i.wall.1@bham.ac.uk (I.B. Wall).

https://doi.org/10.1016/j.jcyt.2024.11.007

prohibitively expensive to scale because of the cells' limited proliferative capacity and complexity adapting to bioreactor systems [21,22].

However, process scaling can directly impact DSP performance. For example, the transition from static culture to dynamic bioreactor culture would introduce numerous agitational forces that may result in greater levels of cell breakage [23] and thus changes to the impurity burdens. Moreover, scale increases will likely uncover previously undetectable impurities (e.g., organelles that may be at concentrations insufficient for detection at smaller scales).

These limitations are compounded by limited rates of EV production [10]. Unlike protein/antibody products, in which production rate can be enhanced, EVs are constitutively expressed products. This inextricably links EV production rates to the cell of origin (although this may change upon development of dedicated EV-producing cell lines). The significance of this is if EVs cannot be readily expressed at greater rates, processes must scale to accommodate larger production, further necessitating studies that reflect future process performance.

Consequently, small-scale studies that are unrepresentative of the future manufacturing process will require recharacterization. For example, studies evaluating EV function with DSP output of scaled cultures will be required. In addition, isolation methods that are not detrimental to product potency will be necessary for understanding EV efficacy to ultimately facilitate commercialization of EVs.

In this study, we used the conditionally immortalized human neural stem cell line CTX0E03 (CTX) [24], which does not suffer the same growth limitations as primary stem cell sources and can produce higher volumes of serum-free human neural stem cell–conditioned medium from scalable cultures [25].

To evaluate the applicability of monolith chromatography purification, we first characterized the CTX cells and the resultant conditioned culture medium (CCM). Using hollow fiber tangential flow filtration (TFF), batches comprising between 3 L and 5 L of conditioned medium were volume reduced into EV-enriched concentrates. We then assessed the EVs in an *in vitro* adult human dermal fibroblast (HDFa) scratch assay to determine the baseline stimulatory effect attributed to the EV concentrate. It has previously been reported that TFF is a scalable method that conserves EV potency [26,27]. Samples were further purified in monoliths and evaluated for both EV product quality attributes (as outlined by International Society for Extracellular Vesicles minimal criteria [28]) and changes to the stimulation of fibroblasts in an *in vitro* scratch assay. As EVs work by binding target cells and delivering biologically active payloads to influence cell activity [3,29,30], we hypothesized that purification-derived damage to EVs would cause reductions in their inherent ability to promote wound repair in this manner.

Methods

CTX cell culture and conditioned medium harvest

CTX cells were grown in T175 flasks coated with Cultrex Mouse Laminin (Trevigen, Gaithersburg, MD, USA). A total of 240 μL of Laminin was diluted in 12 mL of Dulbecco's Modified Eagle's Medium/F12 (Thermo Fisher Scientific, Waltham, MA, USA) (DMEM:F12) and incubated for 1 h at 37°C. Laminin solution was aspirated and replaced by 37 mL of prewarmed reduced modified medium containing growth factors and 4-hydroxytamoxifen (RMM + GF + 4-OHT; recipe provided later).

Cells were seeded at a density of $3–5 \times 10^6$ cells·mL^{-1} and maintained in incubated culture (37°C, 5% carbon dioxide) until 70–80% confluency. Complete medium exchange was performed every 2–3 days until time of passage. To generate sufficient volumes of medium, between 25 and 50 T175 flasks were used per passage.

Conditioned culture medium (CCM) was aspirated and decanted into 50-mL Falcon tubes. CCM was centrifuged (1500 rpm, 5 min) to sediment culture debris. Clarified supernatants were transferred into sterile bottles and stored at −80°C.

During passage, cells were washed with Hanks Balanced Salt Solution without Ca^{2+}/Mg^{2+}, with Phenol Red (Thermo Fisher Scientific). A total of 5 mL of TrypZean/ethylenediaminetetraacetic acid (EDTA) (Lonza, UK) was added per T175 flask and incubated for 5 min at 37° C until cells detached. The enzyme was quenched by an equal volume of Defined Trypsin Inhibitor (Thermo Fisher Scientific) and Benzonase endonuclease (Merck Millipore, Hertfordshire, UK). The cell suspension was centrifuged at 1500 rpm for 5 min. The supernatant was discarded and the cell pellet resuspended in fresh, pre-warmed growth medium. Cells were counted by hemocytometer and Trypan Blue (Thermo Fisher Scientific) staining and reseeded in new T175 flasks.

CTX Growth medium preparation

The RMM + GF + 4-OHT recipe per 500 mL of Dulbecco's Modified Eagle's Medium/F12 was as follows. A total of 12 mL was discarded prior to the addition of 20% human albumin solution (Albunorm 20%; Octapharma, Manchester, UK), 20 mg·mL^{-1} human recombinant transferrin (Merck Millipore), 8.1 mg·mL^{-1} putrescine dihydrochloride (Sigma-Aldrich, St Louis, MO, USA), 10 mg·mL^{-1} human recombinant insulin (Sigma-Aldrich), 20 μg·mL^{-1} progesterone (Sigma-Aldrich), 200 mM L-glutamine (Thermo Fisher Scientific), 20 μg·mL^{-1} sodium selenite (Sigma-Aldrich), 10 μg·mL^{-1} basic fibroblast growth factor (bFGF) (PeproTech, Cranbury, NJ, USA) and 10 μg·mL^{-1} epidermal growth factor (EGF) (PeproTech). The medium was passed through a 0.2-μm filter and 1 mM 4-OHT (Sigma-Aldrich) was added prior to use.

CTX immunolabeling

Cells were fixed in 4% paraformaldehyde (PFA) (Sigma-Aldrich) for 15 min at room temperature. Fixed cells were washed three times with phosphate-buffered saline (PBS) (5 min per wash) (Thermo Fisher Scientific) prior to permeabilization with a solution of 0.1% Triton X-100 (Sigma-Aldrich) in PBS (15 min). Non-specific binding was blocked with a 10% solution of fetal bovine serum (FBS) (Thermo Fisher Scientific) in PBS (room temperature for 1 h). Cells were probed with antibodies for nestin (1:200, mouse anti-human; Merck Millipore), glial fibrillary acidic protein (GFAP) (1:5000, rabbit anti-human; Agilent Technologies, Santa Clara, CA, USA) and β-III tubulin (1:500, mouse anti-human; Sigma-Aldrich) prepared in 1% FBS in PBS. Excess antibody was removed by three PBS washes (5 min each). Cells were then incubated (1 h at room temperature in the dark) with appropriate secondary antibodies at a dilution of 1:200 in 1% FBS in PBS. Secondary antibodies were purchased from Thermo Fisher Scientific: Alexa Fluor 568 (goat anti-mouse) and Alexa Fluor 488 (goat anti-rabbit). Cells were washed three times with PBS (5 min per wash) and counterstained with 1 μM Hoechst 33342 (Sigma-Aldrich) for 2 min prior to image acquisition on an EVOS FL fluorescence microscope (Thermo Fisher Scientific).

TFF of CCM

CCM was concentrated by TFF at ReNeuron. A 0.2-μm cutoff vacuum filter (Thermo Fisher Scientific) was used prior to approximately 100-fold volume reduction using a 300-kDa cutoff Spectrum hollow fiber system (Repligen, Waltham, MA, USA). PBS was used as the exchange buffer.

Ultracentrifugation

The tubes used for all ultracentrifugation steps were Thinwall Ultra-Clear tubes (25 × 89 mm, 38.5 mL; Beckman Coulter, Brea, CA, USA), which were used in the SW 28 Ti rotor of an Optima L-100XP ultracentrifuge (Beckman Coulter). We achieved 100 000 × g in the SW 28 Ti rotor (k-factor = 246, maximum rpm = 28 000, maximum relative centrifugal force = 141 000 × g) by a centrifugal speed of

approximately 23 600 rpm. EV pellets are invisible but will settle in the bottom of the tube for swing out rotors, and the expected sedimentation point can be marked on fixed angle rotors using a lab marker. All operations were performed at 4°C.

Differential ultracentrifugation

Samples were centrifuged at 400 × *g* (10 min), 2000 × *g* (20 min) and 20 000 × *g* (40 min) to remove large debris, debris and fine particulates, respectively, using a 5810 lab centrifuge (Eppendorf, Hamburg, Germany). Supernatants were retained and transferred to fresh tubes. Once clarified, supernatants were transferred to Thinwall Ultra-Clear tubes for ultracentrifugation for 120 min at 100 000 × *g*. Tubes and housing were balanced to ± 0.1 g, brimmed. Maximal braking was used to decelerate the centrifuge upon completion. The supernatant was discarded, and the EV pellet was resuspended in PBS.

Sucrose/heavy water cushion ultracentrifugation

We performed the same clarification steps as for the differential ultracentrifugation (i.e., 400 × *g*, 2000 × *g*, 20 000 × *g*). Then a 30% (w/w) sucrose/heavy water cushion was placed in the ultracentrifuge tube (optimal cushion volume is between one eighth and one sixth of tube volume) (heavy water procured from Sigma-Aldrich). Samples were layered on top of the cushion and then brimmed and balanced to ± 0.1 g. This was ultracentrifuged for 120 min at 100 000 × *g* (minimal braking to decelerate). On completion, the EV-depleted supernatant was removed, leaving only the cushion. The cushion was diluted with PBS until the tube was brimmed and rebalanced to ± 0.1 g and then recentrifuged at 100 000 × *g* for 120 min. Maximal braking was used to decelerate the centrifuge. The supernatant was discarded, and the EV pellet was resuspended in PBS.

Density gradient ultracentrifugation

Density layers were produced by combining iodixanol (OptiPrep; Axis-Shield Density Gradient Media, Oslo, Norway), initially a 60% solution, in a volume ratio of 5:1 with 0.25M sucrose stock solution (containing 60 mM Tris hydrochloride, 6 mM EDTA) to produce a final 50% iodixanol stock (as described in the Axis-Shield application note; www.optiprep.com). This 50% stock was then diluted further (Table 1) using the same 0.25M sucrose stock to create the density gradients used.

Each 2-mL cushion (highest density at the bottom) was layered using a P200 pipette such that the layers settled with minimal mixing. PBS-diluted EV concentrate was loaded on top. Once tubes were brimmed and balanced to ± 0.1 g, ultracentrifugation was performed at 100 000 × *g* for 72 h with no braking to decelerate the centrifuge. Fractions were recovered from the top down. Each like-for-like 2-mL layer was pooled with those of the other tubes, diluted with PBS and recentrifuged at 100 000 × *g* to provide pellets for analysis. The final centrifugation lasted 1 h and applied maximum braking.

Table 1
Composition ratios of iodixanol stock and 0.25M sucrose for isopycnic density gradient preparation.

Fraction, –	Density, g·mL^{-1}	Iodixanol, %	Composition ratio, 10 mL	
			Iodixanol stock	0.25M sucrose
1	1.107	16	3.2	6.8
2	1.117	18	3.6	6.4
3	1.127	20	4.0	6.0
4	1.136	22	4.4	5.6
5	1.146	24	4.8	5.2
6	1.156	26	5.2	4.8
7	1.165	28	5.6	4.4
8	1.175	30	6.0	4.0
9	1.185	32	6.4	3.6
10	1.204	36	7.2	2.8
11	1.243	44	8.8	1.2
12	1.272	50	10.0	0.0

Fraction number corresponds to later Western blot identifier (F1–12). "-" designates a field has no unit.

Monolith chromatography

Two 1-mL, 6-μm-pore Convective Interaction Media monolith columns were purchased from Sartorius, (Gottingen, Niedersachsen, Germany). One was a strong anion exchanger (quaternary amine [QA]) and the other was a hydrophobic interaction column (HIC) with a hydroxyl ligand (OH). Chromatography was performed on an ÄKTA avant liquid chromatography system (GE Healthcare, Uppsala, Sweden).

Both columns used the same general protocol (see later discussion), with differences stemming only from the buffers used for equilibration/sample loading, washing and elution/column stripping. All buffers were sterile filtered (Nalgene Rapid-Flow, 0.22 μm; Thermo Fisher Scientific) and made fresh on the day of use. To prepare buffers, all chemicals were purchased in solid form from Sigma-Aldrich.

General chromatography process

Columns were flushed of the 20% ethanol storage solution using ultrapure, particle-free water (20 column volumes [CV] at 5 CV·min^{-1}). Cleaning-in-place was performed using 1M sodium hydroxide and 2M sodium chloride (NaCl) (15 CV at 0.5 CV·min^{-1}). Columns were flushed with ultrapure, particle-free water (20 CV at 5 CV·min^{-1}). Columns were regenerated using respective elution buffer (20 CV at 5 CV·min^{-1}). Columns were re-equilibrated using respective equilibration/loading buffer (20 CV at 5 CV·min^{-1}). Product was then loaded (TFF concentrate diluted 10-fold by equilibration buffer) at 5 CV·min^{-1}. Columns were then washed using respective equilibration buffer (20 CV at 5 CV·min^{-1}). Elution was performed (either by linear gradient or by step change as required by the specific experiment) using elution buffer or mixtures of elution and equilibration buffer at 2 CV·min^{-1}. Columns were stripped using 100% elution buffer followed by a water rinse (both 10 CV at 5 CV·min^{-1}). Columns were cleaned using 1M sodium hydroxide and 2M NaCl (30 CV at 0.5 CV·min^{-1}) and flushed with equilibration buffer and then ultrapure, particle-free water prior to storage in 20% ethanol (each 20 CV at 5 CV·min^{-1}). Columns were stored at 4°C. The QA loading/equilibration buffer comprised 50 mM Tris (pH 8.0). The QA elution buffer comprised 2M NaCl and 50 mM Tris (pH 8.0). The OH loading/equilibration buffer comprised 2M ammonium sulfate and 50 mM sodium phosphate (pH 7.0). The OH elution buffer comprised 50 mM sodium phosphate (pH 7.0).

Buffer exchange

We purchased 10-kDa Slide-A-Lyzer G2 Dialysis Cassettes from Thermo Fisher Scientific. Cassettes were submerged in sterile PBS until the membranes softened. Samples were aseptically pipetted into the cassettes in a biological safety cabinet (BSC). Once complete, excess air was squeezed gently from the cassettes. Cassettes were closed and placed in sterile beakers containing 700 mL of sterile PBS chilled to 4°C. Beakers were sealed with aluminum foil and magnetically stirred at 4°C. Stirrer speed was adjusted to avoid vortex formation. After 2 h, PBS was replaced with fresh PBS and stirred for another 2 h. A final PBS change was performed prior to leaving the cassettes overnight. Samples were recovered by pipette in a BSC.

Protein quantification

Protein was quantified using the micro bicinchoninic protein assay (Thermo Fisher Scientific) for low concentration protein

samples, whereas for higher concentration protein samples, the Pierce Coomassie (Bradford) protein assay (Thermo Fisher Scientific) was used. Samples were prepared and analyzed per the manufacturer's instructions. Standard curves were generated using the supplied bovine serum albumin standards.

DNA quantification

To quantify DNA, the Quant-iT PicoGreen dsDNA Assay (Thermo Fisher Scientific) was used. Samples were prepared and analyzed per the manufacturer's instructions. Standard curves were generated using the dsDNA standards supplied with the assay.

NanoSight nanoparticle tracking analysis

The NanoSight LM10 (Malvern Panalytical, Malvern, UK) was used for nanoparticle tracking analysis for quantification of particle concentration and size distribution.

The optical flat and top plate were cleaned with 70% ethanol, dried and then cleaned with water (particle-free). To clean the top plate, the solutions were injected into the inlet and allowed to pass through the outlet port. The holes in the base of the top plate were also injected (gently) to ensure removal of previous samples. Care was taken to ensure the plate was fully dried (via compressed air) prior to the addition of water to ensure no ethanol–water "vesicles" remained within the system. The surfaces of the top plate and optical flat were dried with particle-free tissues prior to reassembly. The cleaning procedure was repeated between all samples.

Samples were recorded for 60 s in triplicate. The camera level of all samples was set to 13; however, CCM required a level of 11 because of the sample brightness, which contributed to higher noise than a slight change in camera level [31].

Samples were injected at a concentration of 10^8–10^9 particles/mL (the optimal operational range of the NanoSight). If concentrations were higher than this, samples were serially diluted using particle-free PBS and remeasured. For samples with lower concentrations (e.g., within chromatograms in which few particles had eluted), the samples were measured as normal for an estimated concentration.

Western blots

Pre-cast 10-well, 1.5-mm-thick NuPAGE Novex 4–12% Bis-Tris gels (Thermo Fisher Scientific) were used to perform sodium dodecyl sulfate–polyacrylamide gel electrophoresis using 1× MES buffer (Thermo Fisher Scientific) at a constant voltage of 200 V (approximately 125 mA) in a vertical electrophoresis tank (Thermo Fisher Scientific). A Spectra multicolor protein ladder (Thermo Fisher Scientific), 20 μL per well, allowed monitoring during electrophoresis and transfer stages.

Samples were heated at 90°C for 10 min after mixing 3:1 with 4× sample buffer (Thermo Fisher Scientific). Samples were briefly centrifuged to ensure condensate was returned to the sample. A total of 35 μL was loaded per well.

The gel casing was carefully opened using a metal spatula. A Western blotting sandwich was prepared as follows: filter paper, sodium dodecyl sulfate–polyacrylamide gel electrophoresis gel, polyvinylidene fluoride membrane and filter paper (Thermo Fisher Scientific). All layers (besides the gel) were soaked in methanol prior to assembly. Air bubbles were rolled out.

These layers were enclosed by thick, clean, methanol-soaked sponges and sealed within the Western blot holder to ensure a tight sandwich. A Western blot tank (Bio-Rad Laboratories, Hercules, CA, USA) was used for the transfer. The tank was filled with transfer buffer using a 1-L recipe: 750 mL Milli-Q ultrapure water (Merck Millipore), 250 mL methanol, 14.41 g glycine and 3.03 g Tris (Sigma-Aldrich). A total of 1.5 L of buffer was prepared in advance and refrigerated. We found that 100 V for 1 h was sufficient to transfer one sandwich and a further 20–30 min was required for double transfers.

Table 2
Western blot antibody concentrations and manufacturers.

Antibody	Concentration	Manufacturer
Anti-CD81	1:100	Thermo Fisher Scientific
Anti-CD63	1:100	Thermo Fisher Scientific
Anti-CD9	1:100	Thermo Fisher Scientific
Anti-HSA	1:2500	Abcam
Anti-GM130	1:1000	Abcam
Anti-TSG101	1:1000	Thermo Fisher Scientific
Goat anti-mouse or goat anti-rabbit IgG (H + L) cross-adsorbed secondary antibody, HRP	1:2000, both	Thermo Fisher Scientific, both

HRP, horseradish peroxidase.

Completion was determined by transfer of the multicolored ladder. Once achieved, membranes were incubated and rocked in square Petri dishes with blocking solution (Thermo Fisher Scientific) for 30–60 min. Membranes were washed twice for 5 min using Milli-Q water (maintained face up). Primary antibody was added to antibody solution (Thermo Fisher Scientific) and incubated with the membrane overnight (refrigerated, in the dark, rocked). For a list of antibodies and concentrations, see Table 2.

Membranes were washed three times (5 min per wash) in antibody wash solution (Thermo Fisher Scientific). The secondary antibody was prepared at 1:2500 in antibody solution and incubated at room temperature for 1–2 h. Membranes were then washed three times with wash solution. Immediately before imaging, membranes were incubated (<10 s) with SuperSignal West Femto Maximum Sensitivity Substrate (Thermo Fisher Scientific) and then imaged on an AI600 imaging system (GE Healthcare, Uppsala, Sweden).

Dermal fibroblast culture

HDFa's were purchased from Thermo Fisher Scientific. Cells were maintained between passage two and passage seven for assay use because of reduced growth potential of older cells. Cells were cultured in T75 flasks in medium 106 (or basal medium) supplemented with low serum growth supplement (Thermo Fisher Scientific). This medium and supplement combination is a complete medium referred to as full growth medium (FGM), or the positive control, in the context of the scratch assay.

Cells were seeded at 5×10^3 cells/cm^2 in T75 flasks containing FGM. Passaging occurred at 70–80% confluence using trypsin/EDTA and Defined Trypsin Inhibitor as detachment and quenching reagents, respectively.

Fibroblast scratch assay

HDFa's were resuspended in basal medium and seeded in wells within the culture inserts of 24 micro well scratch assay plates (ibidi, Gräfelfing, Germany) at a density of 4×10^5 cells·mL^{-1}. A total of 70 μL of this suspension was seeded within each insert well, resulting in 28 000 cells per insert well. The surrounding well was fed with 0.5 mL of basal medium. Plates were incubated overnight (37°C, 5% carbon dioxide) to allow cell attachment. Inserts were carefully removed with sterile tweezers in a BSC. The medium was removed and replaced with fresh basal medium, with the exception of the positive control (which contained FGM). Non-control wells were dosed with sample per experimental requirement.

The assay was observed and imaged every 24 h for 3 days per the "area method" [32]. ImageJ software was used to determine the area of the wound by drawing a border around the wound area to obtain

the pixel count. The initial pixel count of the wound was denoted as 100% wound size (A_0). Pixel counts on day 1, day 2 and day 3 (A_n) were used to calculate the percentage healed; specifically, percentage healed = $(1 - (A_n / A_0)) \times 100$. Data are presented as an average of technical triplicates and error as the standard deviation. An example image of the method is given in supplementary Figure 1.

Transmission electron microscopy

Transmission electron microscopy (TEM) samples were diluted (if necessary) to an appropriately low salt solution to minimize image noise. To each carbon-coated formvar 400 mesh copper grid (held by tweezers), a 2- to 4-μL drop of sample was added and then dried under a lamp. Once almost dry, the grid was washed in a drop of water. Residual liquid was drained by filter paper and the wash step repeated using a fresh drop. Finally, the grid was placed on a drop of uranyl acetate and left for 30 s before draining such that only a thin film of liquid remained. The grid was imaged by TEM between $\times$80 000 and $\times$250 000 magnification.

Results and Discussion

CTX and EV characterization

To assess the suitability of monolith chromatography for purifying cell culture–derived EVs for therapeutic use, we first characterized the CTX cell culture.

EVs derive their function from the type and state [33] of the cell of origin [2]. CTX cells proliferate rapidly in culture; however, when grown in the absence of growth factors and 4-OHT, CTX cells undergo growth arrest and differentiate [24]. As EVs derive function from cell state and knowing that neural stem cell–derived EVs can stimulate fibroblast proliferation [34] within *in vitro* scratch wound healing models, we first needed to show that the CTX cells were proliferative and undifferentiated to elicit the desired function for this study.

As proliferative CTX cells have been previously described [24,25] and are known to universally express nestin, a neuroepithelial stem cell protein found on immature nervous system cells [35], we performed immunocytochemistry on CTX cultures to demonstrate the presence of the marker (Figure 1). In addition, we demonstrated that GFAP and β-III tubulin, which indicate the potential lineages of the immature cells, were co-expressed in CTX cells. In supplementary Figure 1, we show the growth data for a CTX expansion campaign that demonstrates the steady population doubling and high viability cultures of the CTX cells.

By combining the outputs of immunocytochemistry (Figure 1) that indicated universal expression of nestin, GFAP and β-III tubulin as well as the lack of differentiated cell phenotypes in the bright-field micrographs (i.e., lack of rosettes or the specific morphology of astrocytes) and the steady rate of doubling (see supplementary Figure 2), we surmised that the cells were maintained in the proliferative state. Next, we sought to define the EVs obtained from CTX culture. To do this, we isolated EVs from conditioned medium using ultracentrifugation.

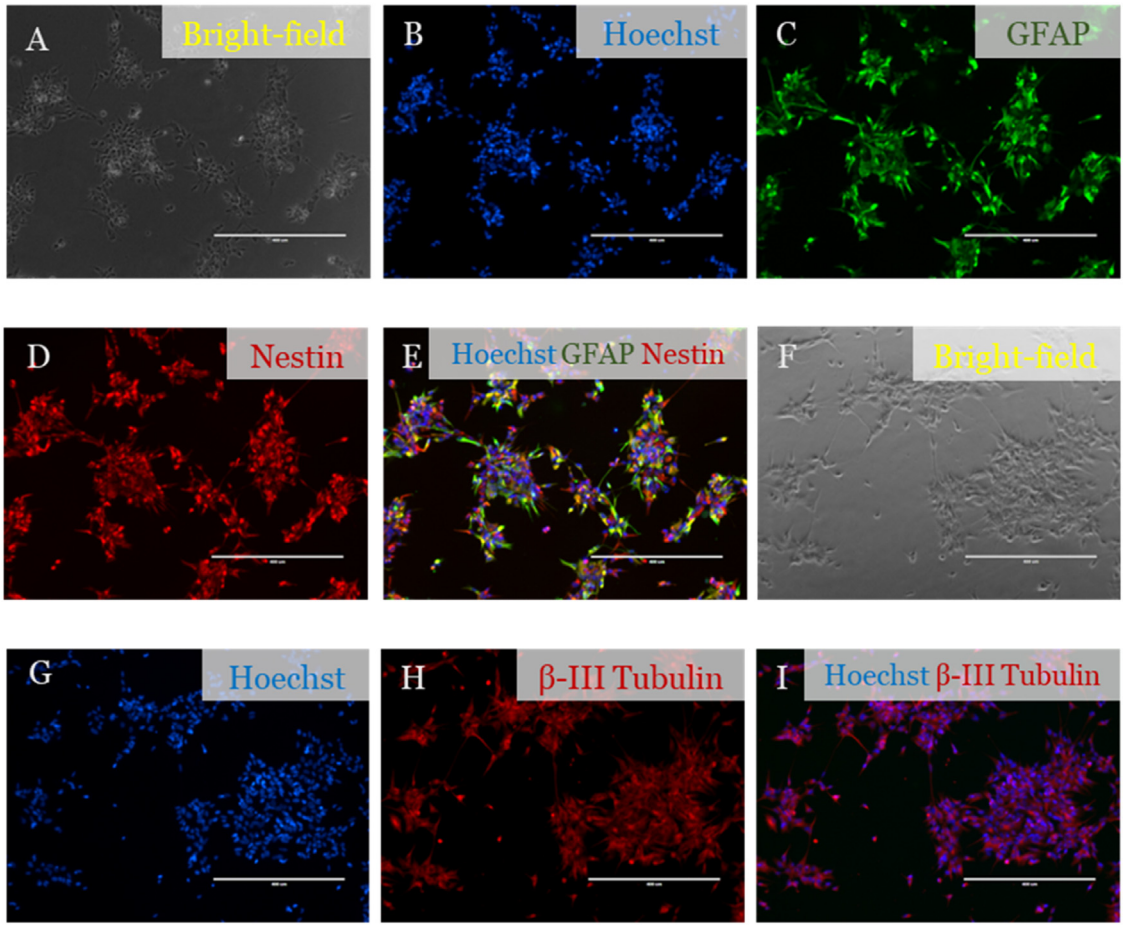

Fig. 1. Proliferative CTX cells are known to be positive for GFAP, nestin and β-III tubulin. Cells were stained to verify the presence of these markers and presented alongside non-fluorescence images. (A) Non-fluorescence image of stained cells in (B-E). (B) Nuclear DNA stain Hoechst (blue). (C) GFAP (green). (D) Nestin (red). (E) Overlay of images (B-E). (F) Non-fluorescence image of stained cells in (G-I). (G) Nuclear DNA stain Hoechst (blue). (H) β-III tubulin (red). (I) Overlay of (G,H). (Color version of figure is available online.)

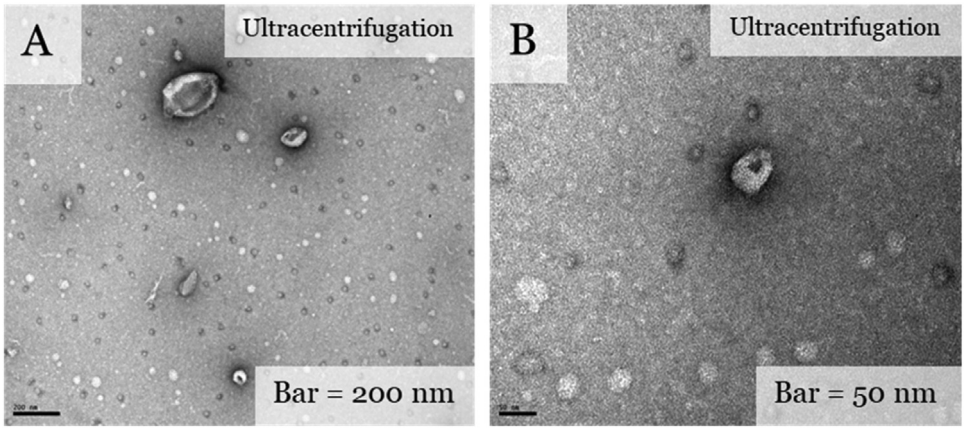

Fig. 2. Transmission electron micrographs of EVs obtained from CTX-conditioned medium. (A,B) EVs obtained from conditioned medium by sucrose cushion differential ultracentrifugation at ×80 000 magnification and ×250 000 magnification, respectively. The EVs display the typical deflated spheroid morphology, with diameters ranging from 50 to 200 nm.

Ultracentrifugation is a frequently reported EV isolation method [7,14]. TEM of CTX-conditioned medium processed with ultracentrifugation revealed the presence of EVs (Figure 2) that presented the typical deflated spheroid morphology (often described as cup-shaped) [36]. However, as EV identification using TEM alone is limited because of the many particulate species found within conditioned culture medium, further analysis was undertaken to define our EVs.

To achieve this, we performed isopycnic (density gradient) ultracentrifugation to elucidate whether our EVs expressed CD81, an EV-associated tetraspanin, and settled within the expected density range of small EVs (1.13–1.19 g·mL^{-1}) as reported in the literature [37–39]. The results of this are presented in Figure 3.

Figure 3A depicts the method used for the isopycnic separation. Density layers were used to fractionate species contained within an EV concentrate (obtained by concentrating 3 L of conditioned medium by TFF). We performed the work using the TFF concentrate because the fractionation did not recover sufficient concentrations of particles from conditioned medium to yield meaningful NanoSight/Western blot results.

Particle size distribution data were obtained from each of the discrete fractions (Figure 3B,C). Notably, in the ribbon plot (Figure 3B), we observed that most particles settled within the desired range of density fractions (1.136–1.185 g·mL^{-1}), whereas fractions beyond this range yielded particle concentrations orders of magnitude lower. In addition, the box plot (Figure 3C) showed that in all fractions the particle size distributions were tightly grouped below 200 nm in diameter, suggesting that no further vesicular aggregation had occurred during the TFF process or the ultracentrifugation. Finally, the fractions from 1.136 to 1.185 g·mL^{-1} contained particles expressing CD81 (Figure 3D). This suggested that TFF concentrates contained high levels of desirable EVs with which to conduct our study. Referring to the minimal criteria for characterizing EVs [28], we could now define desirable EVs from CTX cells as (i) vesicles with a maximum diameter of 150 nm that (ii) express tetraspanins such as CD81 (transmembrane proteins proving the presence of a lipid bilayer structure [28]), (iii) have a flotation density of 1.13–1.19 g·mL^{-1} [40] and (iv) appear as deflated spheroids under TEM [41–43].

Establishing baseline EV functionality

Owing to the proliferative CTX cells used in this study, we expected our EVs to promote wound repair in an *in vitro* HDFa scratch assay. Wound healing by neural stem cell–derived EVs has been shown previously [34]. By using this assay, we could directly measure the stimulatory effect of EVs purified by different methods, as changes to the rate at which wound healing occurred would be indicative of how bioprocessing options affect biological activity. Specifically, as neural stem cell–derived EVs are known to promote fibroblast wound repopulation, reductions in the rate of wound healing would suggest that either the product was being damaged by chromatographic methods or the product identity had changed in a deleterious manner. Conversely, retention of expected healing rates would indicate that the EVs were of the desired identity and able to elicit the biological action of stimulation of fibroblasts.

To validate these claims, we were required to show that the TFF-concentrated EVs could promote wound repair in a dose-responsive manner (Figure 4; also see supplementary Figure 3). To do this, we dosed TFF-recovered EVs (in triplicate) in a scratch assay at 20 μg, 2 μg and 0.2 μg. We also dosed the conditioned medium at 20 μg to compare the effect of the impure medium, in which EVs were unconcentrated and culture proteins were at concentrations desirable for cell proliferation.

The results showed that a 20-μg dose of TFF-concentrated EVs conferred 98.0 ± 1.5% wound healing over 3 days of culture (Figure 4). When reduced to 2 μg and 0.2 μg, the level of wound repair decreased to 71.7 ± 4.9% and 54.9 ± 6.9%, respectively. Wound repair also began immediately, with initial wound healing rates greater than the negative control for all conditions except the conditioned medium.

The reason for this delayed healing in the conditioned meidum sample may be attributed to the composition of the medium itself: although the TFF process had clarified many undesirable particles and some smaller protein species, the conditioned medium was untouched. These artifacts may have caused a deleterious effect or otherwise hindered the immediacy of activity. Alternatively, the fibroblasts may have been adapting to the cell culture components present in the conditioned medium, and thus proliferative excitation took longer to initiate than in EV-enriched samples, in which EVs conferred function by more immediate binding and cellular communication. In a study by Li *et al.* [34], a similar question was asked. In that case, the authors performed an assay using basic fibroblast growth factor (present in their culture medium, as it was in ours) alone dosed at the concentration optimized for cell culture. The authors similarly found that although proliferation was increased, as expected when adding fibroblast growth factor to fibroblast culture, the effect was middling compared with EV-enriched samples.

One limitation of this experiment is that the dosing strategy used the total protein concentration to determine the dose size. One could argue that use of particle counts would be more appropriate; however, even this has several issues. Particle counts are indiscriminate between types of particles and can measure protein aggregates and

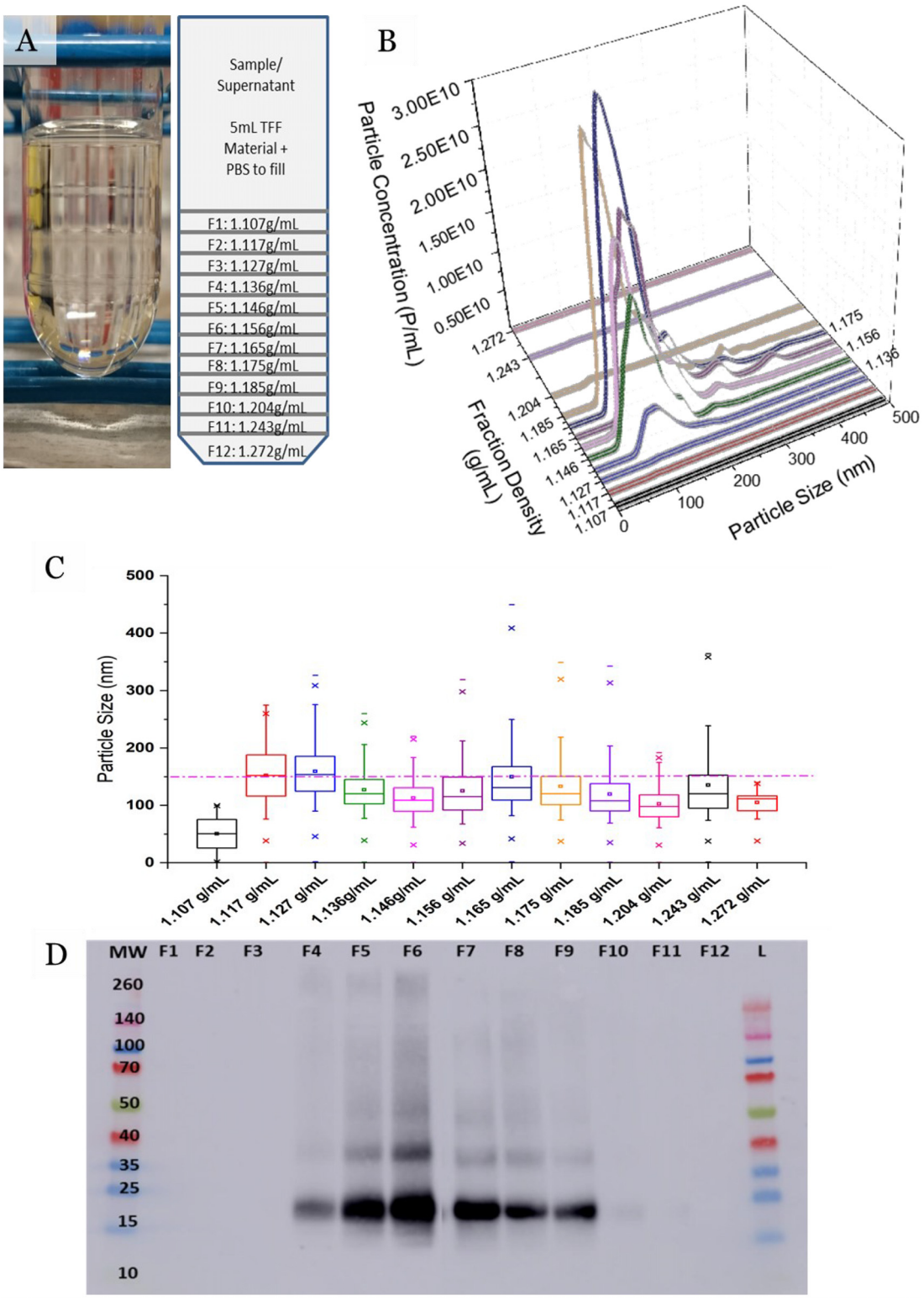

Fig. 3. Characterization of CTX-derived EVs by isopycnic ultracentrifugation. (A) Photograph of layered density gradients presented alongside a diagram of the ultracentrifugation method. (B) Ribbon plot (as determined by NTA NanoSight) demonstrating the particle sizes (nm) and concentrations ($P{\cdot}mL^{-1}$) obtained in each discrete density fraction. (C) Box plot of particle size distribution data for each discrete density fraction. Max value denoted by –, first and 99th percentile values denoted by × and mean values denoted by □. Boxes represent 25th, 50th and 75th percentiles. Whiskers denote min/max values, beyond which are outliers. Pink dashed line represents the max cutoff for desirable EVs at 150 nm. (D) Western blot probing for CD81 across the discrete density fractions comprising two individual Western blots presented side by side (meeting between F6 and F7). Density fractions are designated F1–12 and correspond to the fraction order given by the (C) x-axis. max, maximum; min, minimum; MW, molecular weight; NTA, nanoparticle tracking analysis. (Color version of figure is available online.)

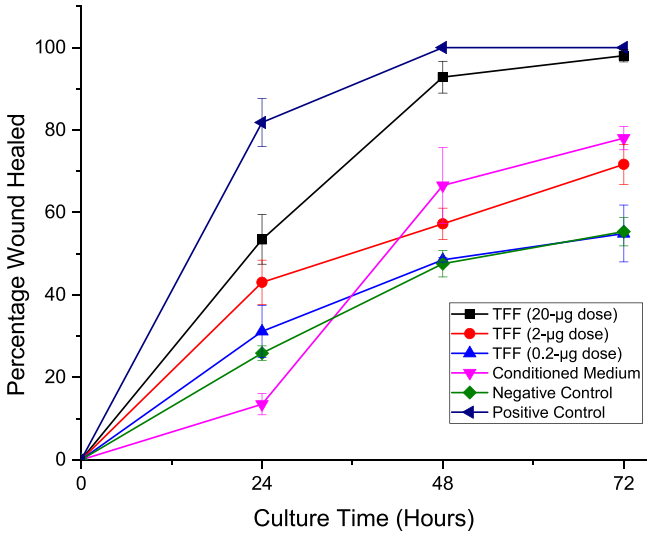

Fig. 4. HDFa wound healing assay characterization. EVs from large-scale CTX culture were concentrated by TFF. Optimal dosing for complete wound repair over 72 h was obtained by dosing EV concentrate at 0.2 μg, 2 μg and 20 μg. A sample of conditioned medium (20-μg dose) was also compared. The positive control was FGM for the fibroblasts to show the optimal growth rate of the cells. The negative control was the non-supplemented medium (i.e., medium 106) to show the minimum proliferative capacity of the HDFa's. Error bars are given as ± standard deviation of triplicate results. (Color version of figure is available online.)

salts that become excited by the laser. To avoid this issue, we selected total protein concentration but presented the results with an approximation of EV-derived protein and the number of particles dosed in the experiment.

Webber and Clayton [44] established that the ratio of particles to protein is a simple but effective method by which to describe EV purity. The article by Webber and Clayton that proposed this method used ultracentrifugation to determine values for high-, mid- and low-purity vesicles from a variety of starting materials. The limitation of this (also mentioned by the authors) was that ultracentrifugation would certainly recover non-EV particles and protein aggregates presenting as particles. Using the value for high-purity EV preparations given (approximately 10^{10} P·μg^{-1} of protein) and assuming that the impurity contribution was negligible allowed us to estimate the EV-derived protein content by taking the reciprocal value and multiplying by the number of particles dosed. Doing so allowed us to compare the effective EV protein content per dose. These values are summarized in Table 3.

This showed us that the conditioned medium contained a relatively low EV-derived particle dose. Despite this, we observed that the effect of wound repair was comparable to the 2-μg dose of TFF material (78.0% compared with 71.7%), which shared a similar magnitude of EV-derived protein.

By extension, we concluded that function was most likely derived from the EVs and not the culture-associated protein, as the conditioned medium was composed of 1.05% EV-derived protein, whereas the 20-μg dose of TFF-recovered EVs consisted of 24.5% EV-derived protein. As we have shown that wound healing is dose-responsive, one would expect that if culture protein were the main contributor to function the conditioned medium would outperform the TFF dose because of its higher culture protein content.

Finally, we demonstrated the assay performance of two ultracentrifugation processes for recovering EVs from conditioned medium: a standard differential ultracentrifugation and one that included a 30% sucrose/heavy water cushion step (see supplementary Figures 4, 5). As expected, we observed that the use of the cushion improved EV purity (the cushion excludes species that cannot sediment within it). Additionally, stimulation was affected positively by this improvement in purity. However, neither process matched the TFF concentrate in performance. These results align with literature observations that demonstrate that ultracentrifugation alone may retain high levels of co-isolating impurities that mask/impair EV function [45] and that claim that ultracentrifugation causes damage to the EVs [17,46]. As we have shown that the sucrose cushion provided purer EV preparations, our results align with this idea of deleterious co-isolation. The fact that neither ultracentrifugation step achieved healing comparable to TFF-recovered EVs (despite comparable EV-derived protein mass in the sucrose cushion step) suggests that some damage to the final cushionless 100 000 × g pellet in both processes may impair EV function.

Monolith chromatography for EV purification

Having characterized the EVs, we sought to evaluate the applicability of monolith chromatography for EV purification. Of the available options, we selected a QA and HIC monolith with a hydroxyl ligand (OH). QA processes have been reported in the literature, albeit for raw conditioned medium [47]. In our study, we discovered that the major species recovered by TFF (EVs/particulates, culture-derived protein, free DNA) eluted across the entirety of the elution range (0–1M NaCl) (see supplementary Figure 6). As all species eluted across the entire range (with the largest elution phenomena occurring within 0–200 mM NaCl), we sought to determine whether there was resolution between these species in this range. To do this, we performed a shallow linear gradient between 0 and 200 mM (Figure 5) and found that culture protein (more specifically human albumin that co-isolated with EVs during TFF) initially eluted at 120 mM, whereas EVs eluted at 140 mM. Although this did not remove the vast majority of co-isolated protein, it did allow some depletion of the proteinaceous burden. Additionally, Benzonase pre-treatment could be used to reduce DNA impurity in the product. However, with such pre-treatment we would later have to verify whether the EV function was unaffected.

We then determined the applicability of a novel OH process (utilizing decreasing ammonium sulfate as the elution method) for EV purification. A recent review reported on chromatographic methods that hold potential for EV purification; however, hydrophobic interaction chromatography was only briefly mentioned [48]. In this review article [48], the HIC processes discussed typically used weak hydrophobic exchangers and the polymer poly(ethylene terephthalate), as reported in Wang et al. [49]. Interestingly, these polymer-

Table 3
Summary of sample metrics for dose–response scratch assay.

Sample	Purity$_{(Protein)}$, P·μg^{-1}	Particles per dose, –	Equivalent EV-derived protein mass, 2 S.F., μg	Wound healed after 72 h, %
TFF, 20 μg	2.44×10^9	4.88×10^{10}	4.9	98.0
TFF, 2 μg	2.44×10^9	4.88×10^9	0.49	71.7
TFF, 0.2 μg	2.44×10^9	4.88×10^8	0.049	54.9
Conditioned medium, 20 μg	1.02×10^8	2.05×10^9	0.21	78.0

Purity (ratio of particles to protein mass) is shown for conditions tested in the dose–response scratch assay. The equivalent EV-derived protein mass is provided for completeness. "-" designates a field has no unit.
S.F., significant figures.

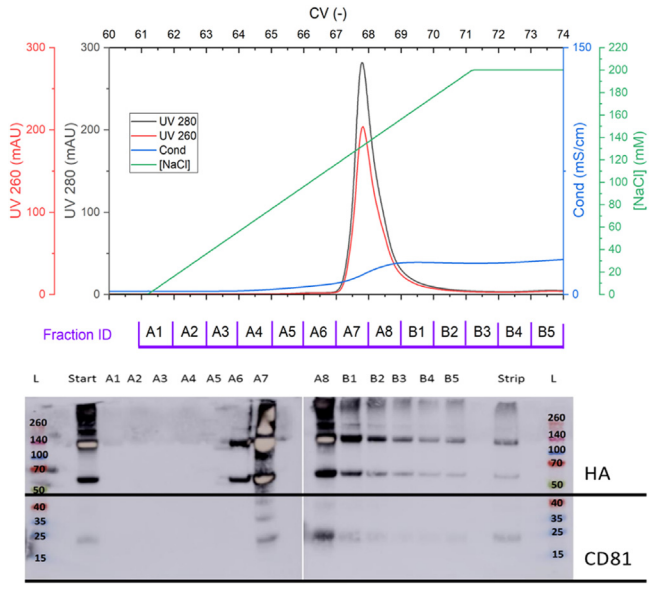

Fig. 5. Characterization of QA monolith process. TFF-recovered EVs were further purified on a QA anion exchange monolith (1-mL CV, 6-μm pore size). To determine whether there was resolution between EVs and the commonly present HA protein in the medium, we performed a linear elution between 0 and 200 mM NaCl. The results showed that elution began at sample A6 (120 mM NaCl) and continued until 200 mM. Overlaid with this was a double Western blot probing for HA and CD81. We observed that some HA was removable by washing at 120 mM but that most of the markers overlapped from 140 mM onward. Cond, conductivity; HA, human albumin; ID, identifier; UV, ultraviolet. (Color version of figure is available online.)

based methods are reminiscent of the poly(ethylene glycol) processes applied by many size exclusion kits to precipitate EVs from solution; however, these kits have often been found to yield impure EV products and are limited in scalability [50]. Moreover, salts such as ammonium sulfate are simpler to remove than long chain polymers, as they more readily pass through buffer exchange processes.

We predicted that the OH–ammonium sulfate system would recover EVs under the hypothesis that, like virus-like particles, a vesicle would possess hydrophobic patches to bind the column. Chromatographic theory suggested that free DNA would not bind the column, whereas albumin would bind in only low amounts (if at all) because of both species' hydrophilic natures.

We also demonstrated the elution profile of the OH process, overlaying the online and assay-based chromatograms with a heat map of NanoSight measurements for all 42 elution fractions obtained (Figure 6A). The trends observed mapped onto one another and showed that a high number of particles were recovered in the latter half of the elution (from 1 to 0M ammonium sulfate). The results also confirmed that DNA was baseline throughout the elution and that the protein content was greatly lowered, with the remaining protein deriving predominantly from the particles. The particle size distributions obtained during elution also suggested that there were no untoward precipitation events occurring, as the particles remained consistent with the expected 150-nm size range of particles.

To confirm the identity of the particles recovered, we performed the processes as might be used in manufacturing scenarios (with a 1.2M wash prior to a 0M elution) and also performed Western blots, probing for albumin, CD81 and CD63. The results (Figure 6B) showed that although the albumin band (69 kDa) was reduced (although some polymers/aggregates persisted), the EV-associated tetraspanins remained unchanged in intensity, verifying successful purification. This suggests that the OH process holds promise for high-purity recovery of EVs from TFF concentrates and should be further researched.

In traditional bioprocessing, multiple chromatographic steps may be used to provide high-purity products. Thus, we performed a combined three-step process of TFF, QA and OH chromatography. To highlight the product retention and impurity removal across the process, we expanded our Western blot panel to cover the four types of markers for EV characterization given in minimal information for studies of EVs guidelines (Figure 7). The first three blots indicated that desirable tetraspanins (CD81, CD63, CD9) were conserved. The next blot (pertaining to the membrane-binding protein TSG101) showed that, although lower in concentration (hence the increased image exposure time for ease of visibility and thus the darker ladder/background), faint bands were observed, indicating EVs possessing a membrane-binding protein. We noted that the expected band size for TSG101 is approximately 50 kDa but that the process yielded an increasing polymer ratio, which was possibly the result of residual salts interfering with the blot protocol. Finally, we probed for two impurity types: albumin (culture medium–derived) and GM130 (a Golgi marker showing the presence of cell-derived organelles/particulates in the retentate). Here we saw that both impurity types were greatly reduced by the end of the process. The reduction in GM130 verified that the particle counts were not entirely EV-based, as organelles were present as particulates. Thus, further methods of estimating EV ratios, such as ELISA or assay-based methods, are critical for EV process output characterization.

As our study related to post-purification function, we then tested our hypothesis that monolith purification conserved the EVs' capacity to stimulate fibroblast wound repair. To do this, we compared the products of two processes, including their intermediate products. The first process purified the TFF concentrate on the QA column prior to OH. The second process reversed this and performed OH purification prior to the QA step (in case one step damaged the EVs). All processes used the same batch of TFF concentrate for comparability.

Because the 1-mL columns had varying capacities related to the level of co-isolation observed, we performed multiple QA steps to recover sufficient material to test and load onto the OH column (however, both processes began with 4 mL of TFF concentrate). Although less indicative of a routine manufacturing process, the experimental design allowed for full analytical testing of the intermediate products.

The results are given in Table 4 and show that monolith purification yielded greater purities in terms of particle-to-protein and particle-to-DNA ratios compared with the TFF concentrate. Additionally, we demonstrated the particles per 20-μg dose related to the scratch assay, the results of which are shown in Figure 8. Western blots for both processes are given in supplementary Figure 7, with representative scratch assay images provided in supplementary Figure 8.

Regarding product performance, we found that wound repopulation was generally conserved across the purification process with comparable results to the originating TFF material, with only the TFF + OH + QA process being statistically different from the other samples ($P < 0.05$). However, of the samples assayed, TFF + OH + QA was the only one to have a replicate that could be considered anomalous, individually yielding 92.2%, 76.3% and 90.1% healing. This errant replicate reduces an otherwise 91% average and increases the spread of the results, contributing to the shift toward significance. We do not believe that the lower outputs of the QA ending processes are indicative of process-associated damage, as it is illogical to presume that the subsequent OH step could repair this. Notably, all samples processed were statistically significant against the negative control, with P values ranging between $\times 10^{-7}$ and $\times 10^{-8}$. A graph highlighting the statistical significance of the results is given in supplementary Figure 9.

These results serve to verify that the wound repair was EV-derived. We found that the relative level of EV-associated protein doubled (after three rounds of purification intentionally targeting the removal of non-EV species), with no major variation in the output. If culture protein were the true functional entity, and considering the dose responsiveness of the assay, one would expect depleted functional output.

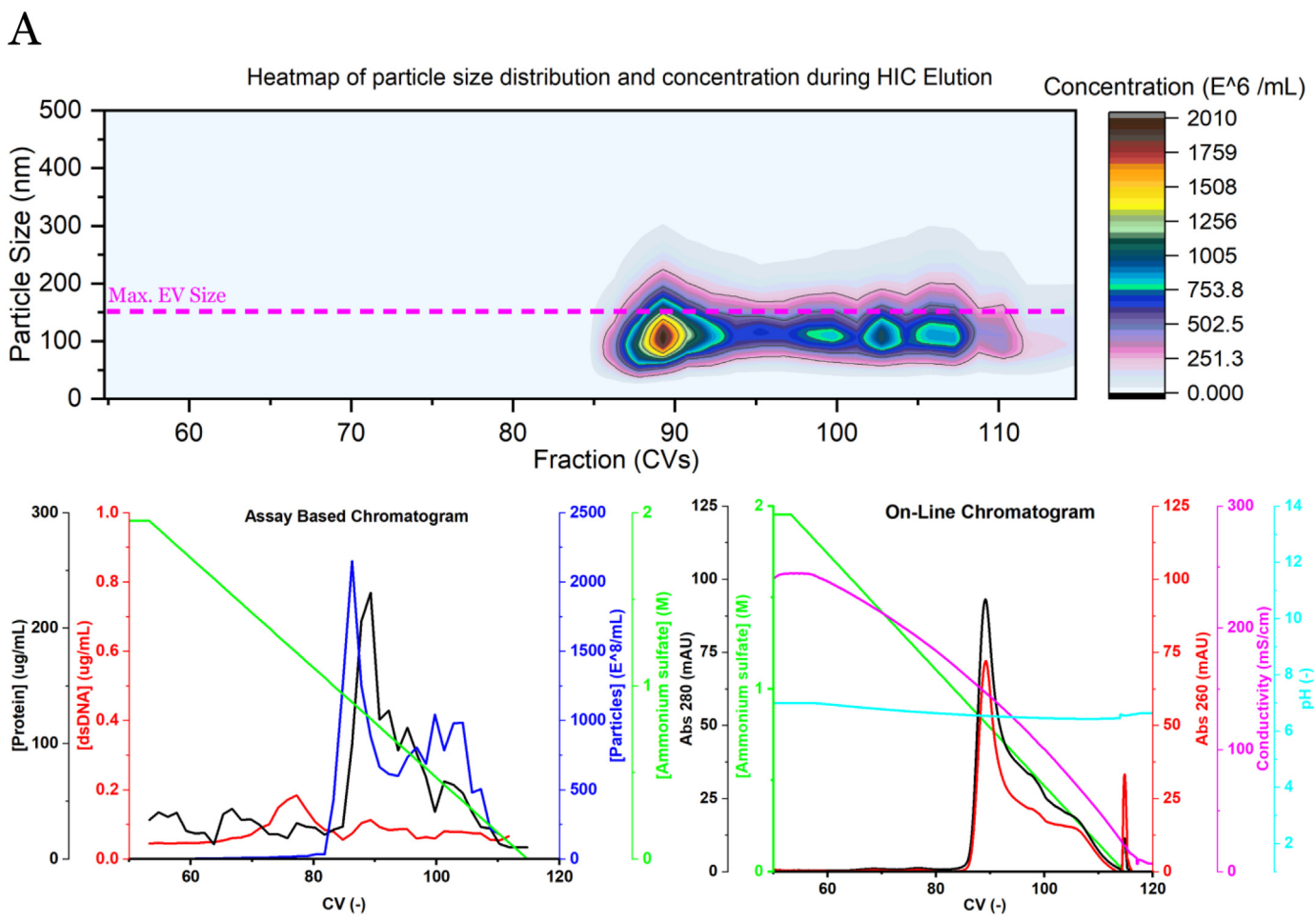

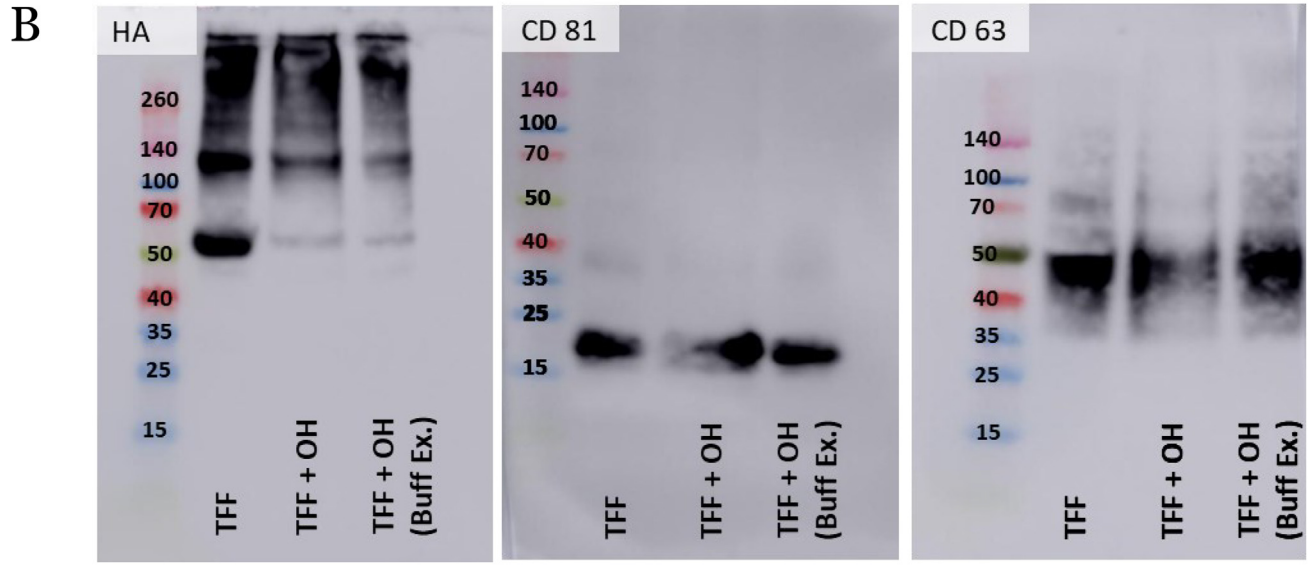

Fig. 6. Characterization of OH monolith process. TFF-recovered EVs were purified on an HIC monolith with OH ligand (1-mL CV, 6-μm pore size). (A) Heat map of particle size data and elution of 42 fractions (upper), with assay-based (protein, DNA and NanoSight) and online (absorbance at 280 nm and 260 nm, AS concentration, conductivity [mS/cm] and pH) measurements (lower). (B) Three Western blots (equal volume loading to allow intensity comparisons) to highlight the purification output (TFF-concentrated EVs were eluted at 0M AS after a wash at 1.4M AS). Buff Ex. with fresh PBS was performed to remove residual AS, which interferes with Western blots. The next blots highlighted conservation of the desirable EV markers CD81 and CD63. AS, ammonium sulfate; Buff Ex., buffer exchange; HA, human albumin. (Color version of figure is available online.)

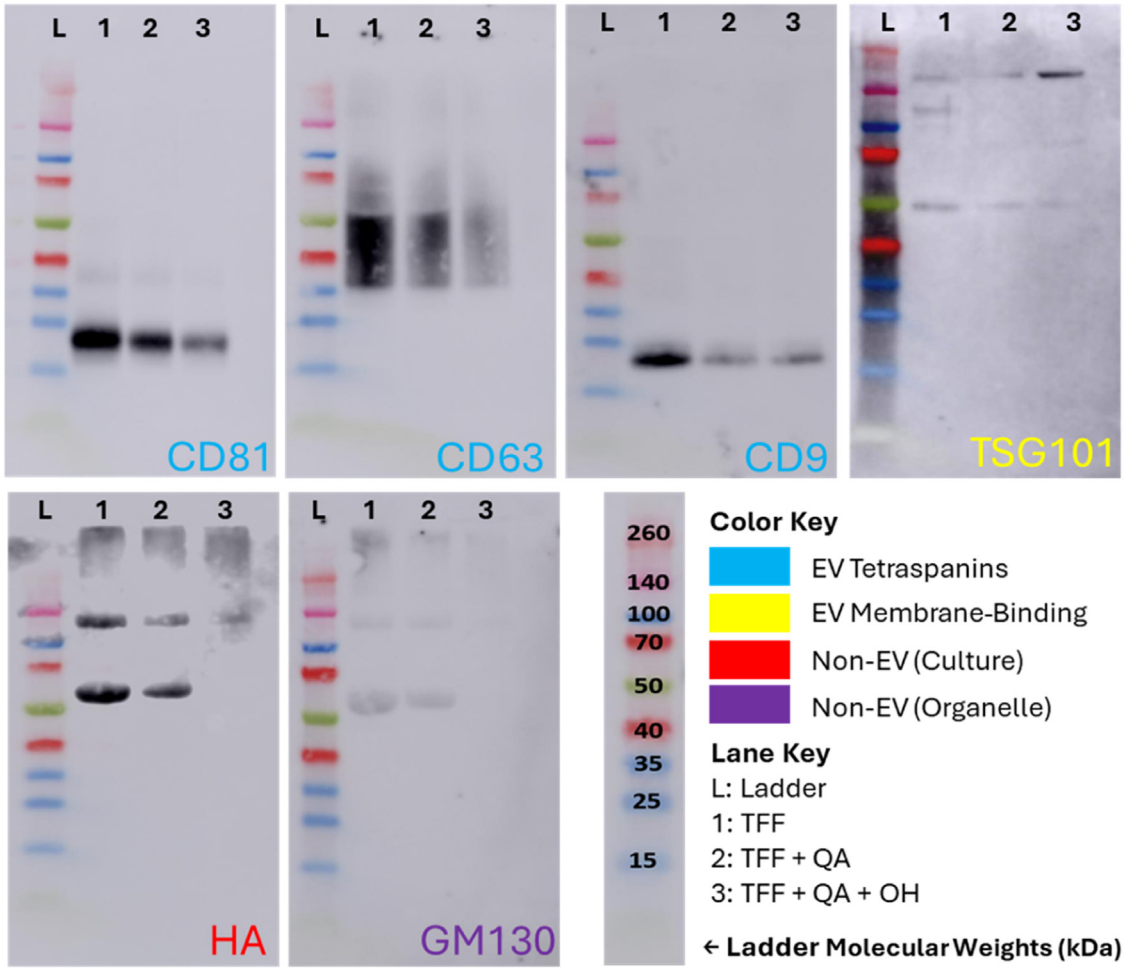

Fig. 7. Western blots of EVs purified by monolith chromatography. EVs from large-scale CTX culture were concentrated by TFF and then purified by QA and OH monoliths (1-mL CV, 6-μm pore size). Blots were loaded with equal volume to allow visual comparison of intensity. The top row of blots shows the EV identification markers (tetraspanins CD81, CD63 and CD9) and TSG101 (demonstrating that EVs possess membrane-binding potential). For TSG101, image exposure was increased to improve visibility. The second row shows HA (culture medium–derived impurity) and GM130 (Golgi marker proving the presence of culture-derived organelles). HA, human albumin. (Color version of figure is available online.)

One limitation of this study is that the purified doses provided an excess of EVs compared with the TFF concentrate (7–10 μg compared with 4.9 μg of EV-associated protein) because of the dosing method (20 μg of total protein per sample). Although this could be interpreted to suggest that a higher EV dose at greater purity could only match the TFF material, we must also consider that overdosing the cells with EVs or other proliferative stimulus is unlikely to yield faster wound coverage than the positive control, as the cells are physically limited to doubling in a certain time.

Finally, we acknowledge that this research is limited to a single EV type and one non-specific assay. We recommend further investigations to explore a wider variety of EVs and assays to validate our discovery. However, these findings are still important to EV manufacturing prospects, as they demonstrate that monolith chromatography (a well-characterized biotechnology process) can remove impurities commonly found in EV products while likely conserving product function/integrity. Were the EVs unable to bind and deliver functional payloads via damage or other deleterious side effect, and considering the dose-responsive nature of the results, there would be no reason for the maintained levels of wound repair observed. As such, we believe that development of these processes could drastically improve upon the current state of the art of EV bioprocessing and facilitate EV process commercialization.

Conclusions

We have shown that EVs can be purified from TFF concentrates by anion exchange (QA) and hydrophobic interaction (OH) monolith chromatography. The QA column resulted in overlapping elution of EV and DNA/culture protein, which limits its use with cruder process streams. However, the column could find use within a larger DSP train in combination with more specific primary recovery options (e.g., an affinity column). The OH column outperformed the QA column, with a strong preference of the column to bind EVs while forgoing the co-isolation of culture proteins, DNA and GM130, suggesting the removal of organelle-based particulates.

Both columns were tested, alone and in combination, to determine how column chromatography impacts EV performance using an *in vitro* fibroblast scratch assay. The results indicated that no major differences in wound healing were observed with one- or two-step purification processes of the TFF material. This contrasted with ultracentrifugation, in which EVs failed to promote wound closure over the 72-h assay period, suggesting functional losses.

The study has shown that EVs retain their functional activity after monolith chromatography; a process which also benefits from being more scalable and translatable than ultracentrifugation. The QA column held approximately 1 mL of 100× EV concentrate. As monoliths can be as large as 2 L, a column could theoretically hold the

Table 4
Comparative purity ratios of monolith-purified EVs.

Sample	Purity$_{(Protein)}$, P·μg^{-1}	Purity$_{(DNA)}$, P·μg^{-1}	Particles per 20-μg dose, –	Equivalent EV-derived protein mass, 2 S.F., μg	Wound healed after 72 h, %
TFF	2.44×10^{9}	1.88×10^{11}	4.88×10^{10}	4.9	98.0
TFF + QA	5.00×10^{9}	3.88×10^{11}	1.00×10^{11}	10	90.8
TFF + QA + OH	4.10×10^{9}	1.75×10^{12}	8.21×10^{10}	8.2	98.0
TFF + OH	3.97×10^{9}	3.12×10^{12}	7.95×10^{10}	7.9	96.4
TFF + OH + QA	3.79×10^{9}	2.50×10^{12}	7.58×10^{10}	7.6	86.2

TFF-recovered EVs were further purified by monolith chromatography. Purity ratios of particles with respect to protein and DNA are shown. In addition, the equivalent EV-associated dose was calculated and is shown alongside wound repair observed in *in vitro* scratch assay. "-" designates a field has no unit.
S.F., significant figures.

equivalent of 200 L of conditioned medium that has been similarly processed by TFF. If this feed were optimized to reduce the level of co-binding impurities, this scale could increase even further. For context, the OH column held at least three times the volume of TFF concentrate compared with the QA column, with no breakthrough limit determined. (These monoliths have capacities of greater than $10^{12–14}$ P·mL^{-1}, which aligns with our QA column, which accommodated 1.88×10^{12} particles from the TFF feed.)

This shows that the potential for a scalable, translatable DSP train aligned with biopharmaceutical processing exists for EV products. Such a process may look like the following: bioreactor culture → TFF concentration/wash → affinity chromatography → QA intermediate → OH polish → buffer exchange/formulation.

We also highlighted limitations in the metrics used to describe EV purity. By demonstrating that at larger scales of high- viability, flask-based culture organelles such as Golgi become detectable in EV products, we emphasized the necessity for DSP methods that can actively remove these impurities.

Finally, we showed that further studies on material characterization will be needed as EVs progress toward clinical manufacture. Critically, as EV process scales increase, we will find that impurities (which may otherwise present as EVs) become more evident. Our study has evidenced how co-isolation can skew purity measurements and wound healing assay readouts, which in turn may alter how product characterization is interpreted. Thus, multi-dimensional analyses of EV products are required to ensure these therapeutic candidates are thoroughly described as required by industry and regulation.

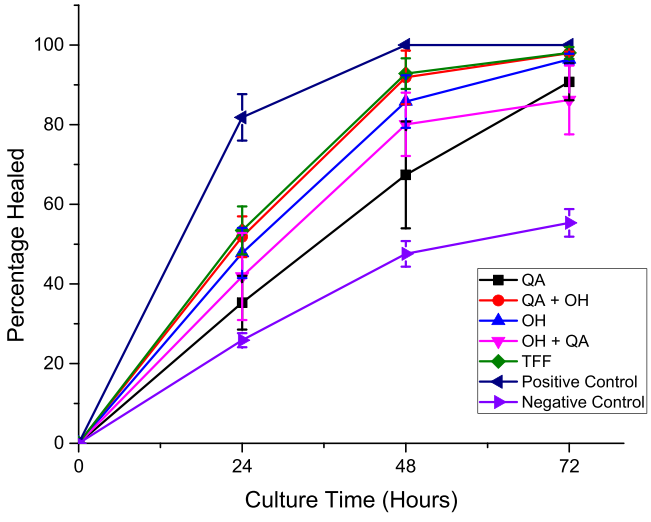

Fig. 8. Assessment of stimulatory outputs for monolith-purified EVs. TFF-recovered EVs were purified further by monolith chromatography. Samples were purified by QA and OH monoliths, alone or in combination, to mimic steps within a larger DSP train. All samples were dosed at 20 μg (total protein). The positive control is the complete growth medium (FGM) for the fibroblasts. The negative control is the non-supplemented medium (i.e., medium 106). Error bars are given as ± standard deviation of triplicate results. (Color version of figure is available online.)

Funding

This research received funding from the Engineering and Physical Sciences Research Council Industrial Doctoral Training Centre in Bioprocess Engineering Leadership (grant no. EP/G034656/1) and ReNeuron Ltd.

Declaration of Competing Interest

The authors have no commercial, proprietary or financial interest in the products or companies described in this article.

Author Contributions

Conception and design of the study: ILC, RLC, DGB and IBW. Acquisition of data: ILC. Analysis and interpretation of data: ILC, RLC, DGB and IBW. Drafting or revising the manuscript: ILC, RLC, DGB and IBW. All authors have approved the final article.

Acknowledgments

ILC, DGB and IBW wish to acknowledge ReNeuron Ltd. for its collaboration and generous provision of materials.

Supplementary materials

Supplementary material associated with this article can be found in the online version at doi:10.1016/j.jcyt.2024.11.007.

References

[1] de Abreu RC, et al. Native and bioengineered extracellular vesicles for cardiovascular therapeutics. Nature Reviews Cardiology 2020;17:685–97.
[2] Lener T, et al. Applying extracellular vesicles based therapeutics in clinical trials—An ISEV position paper. J Extracell Vesicles 2015;4:1–31.
[3] El Andaloussi S, Mäger I, Breakefield XO, Wood MJA. Extracellular vesicles: Biology and emerging therapeutic opportunities. Nature Reviews Drug Discovery 2013;12:347–57.
[4] Meng W, et al. Prospects and challenges of extracellular vesicle-based drug delivery system: considering cell source. Drug Deliv 2020;27:585–98.
[5] Elsharkasy OM, et al. Extracellular vesicles as drug delivery systems: Why and how? Advanced Drug Delivery Reviews 2020;159:332–43.
[6] Herrmann IK, Wood MJA, Fuhrmann G. Extracellular vesicles as a next-generation drug delivery platform. Nature Nanotechnology 2021;16:748–59.
[7] Colao IL, Corteling R, Bracewell D, Wall I. Manufacturing Exosomes: A Promising Therapeutic Platform. Trends Mol Med 2018;24:242–56.
[8] Ahn SH, et al. Manufacturing Therapeutic Exosomes: from Bench to Industry. Mol Cells 2022;45:284–90.
[9] Rohde E, Pachler K, Gimona M. Manufacturing and characterization of extracellular vesicles from umbilical cord–derived mesenchymal stromal cells for clinical testing. Cytotherapy 2019;21:581–92.
[10] Erwin N, Serafim MF, He M. Enhancing the Cellular Production of Extracellular Vesicles for Developing Therapeutic Applications. Pharmaceutical Research 2023;40:833–53.

[11] Turano E, Scambi I, Virla F, Bonetti B, Mariotti R. Extracellular Vesicles from Mesenchymal Stem Cells: Towards Novel Therapeutic Strategies for Neurodegenerative Diseases. International Journal of Molecular Sciences 2023;24:1–20.
[12] Zhang Y, et al. Therapeutic Role of microRNAs of Small Extracellular Vesicles from Human Mesenchymal Stromal/Stem Cells in Treatment of Experimental Traumatic Brain Injury. J Neurotrauma 2023;40:758–71.
[13] Dimik M, Abeysinghe P, Logan J, Mitchell M. The exosome: a review of current therapeutic roles and capabilities in human reproduction. Drug Delivery and Translational Research 2023;13:473–502.
[14] Gardiner C, et al. Techniques used for the isolation and characterization of extracellular vesicles: Results of a worldwide survey. J Extracell Vesicles 2016;5:1–6.
[15] Liangsupree T, Multia E, Riekkola ML. Modern isolation and separation techniques for extracellular vesicles. J Chromatogr A 2021;1636:1–17.
[16] Kimiz-Gebologlu I, Oncel SS. Exosomes: Large-scale production, isolation, drug loading efficiency, and biodistribution and uptake. Journal of Controlled Release 2022;347:533–43.
[17] Mol EA, Goumans MJ, Doevendans PA, Sluijter JPG, Vader P. Higher functionality of extracellular vesicles isolated using size-exclusion chromatography compared to ultracentrifugation. Nanomedicine 2017;13:2061–5.
[18] Fernández-Rhodes M, et al. Defining the influence of size-exclusion chromatography fraction window and ultrafiltration column choice on extracellular vesicle recovery in a skeletal muscle model. Journal of Extracellular Biology 2023;2:1–18.
[19] Grangier A, et al. Technological advances towards extracellular vesicles mass production. Advanced Drug Delivery Reviews 2021;176:1–16.
[20] Luo Z, Chen Y. Unlocking Delivery Strategies for mRNA Therapeutics. Recent Pat Anticancer Drug Discov 2024;19:126–9.
[21] Ahn SH, et al. Manufacturing Therapeutic Exosomes: from Bench to Industry. Mol Cells 2022;45:284–90.
[22] Mas-Bargues C, Borrás C. Importance of stem cell culture conditions for their derived extracellular vesicles therapeutic effect. Free Radic Biol Med 2021;168:16–24.
[23] Tsai HH, Yang KC, Wu MH, Chen JC, Tseng CL. The effects of different dynamic culture systems on cell proliferation and osteogenic differentiation in human mesenchymal stem cells. Int J Mol Sci 2019;20:1–14.
[24] Pollock K, et al. A conditionally immortal clonal stem cell line from human cortical neuroepithelium for the treatment of ischemic stroke. Exp Neurol 2006;199:143–55.
[25] Thomas RJ, et al. Automated, serum-free production of CTX0E03: A therapeutic clinical grade human neural stem cell line. Biotechnol Lett 2009;31:1167–72.
[26] Haraszti RA, et al. Exosomes Produced from 3D Cultures of MSCs by Tangential Flow Filtration Show Higher Yield and Improved Activity. Molecular Therapy 2018;26:2838–47.
[27] Lee JH, et al. Reproducible large-scale isolation of exosomes from adipose tissue-derived mesenchymal stem/stromal cells and their application in acute kidney injury. Int J Mol Sci 2020;21:1–16.
[28] Théry C, et al. Journal of Extracellular Vesicles Minimal information for studies of extracellular vesicles 2018 (MISEV2018): a position statement of the International Society for Extracellular Vesicles and update of the MISEV2014 guidelines. J Extracell Vesicles 2018;7:1–43.
[29] Théry C, Zitvogel L, Amigorena S. Exosomes: Composition, biogenesis and function. Nature Reviews Immunology 2002;2:569–79.
[30] Hur YH, Cerione RA, Antonyak MA. Extracellular vesicles and their roles in stem cell biology. Stem Cells 2020;38:469–76.
[31] Maas SLN, et al. Possibilities and limitations of current technologies for quantification of biological extracellular vesicles and synthetic mimics. Journal of Controlled Release 2015;200:87–96.
[32] Bobadilla AVP, et al. *In vitro* cell migration quantification method for scratch assays. J R Soc Interface 2019;16:1–11.
[33] Kusuma GD, et al. Effect of 2D and 3D Culture Microenvironments on Mesenchymal Stem Cell-Derived Extracellular Vesicles Potencies. Front Cell Dev Biol 2022;10:1–17.
[34] Li J, et al. Enhancing Cutaneous Wound Healing Based on Human Induced Neural Stem Cell-derived Exosomes. Int J Nanomedicine 2022;17:5991–6006.
[35] Zhang J, Jiao J. Molecular Biomarkers for Embryonic and Adult Neural Stem Cell and Neurogenesis. BioMed Research International 2015;2015:1–14.
[36] Malenica M, et al. Perspectives of microscopy methods for morphology characterisation of extracellular vesicles from human biofluids. Biomedicines 2021;9:1–29.
[37] Zonneveld MI, et al. Recovery of extracellular vesicles from human breast milk is influenced by sample collection and vesicle isolation procedures. J Extracell Vesicles 2014;3:1–12.
[38] Nguyen HPT, Simpson RJ, Salamonsen LA, Greening DW. Extracellular vesicles in the intrauterine environment: Challenges and potential functions. Biol Reprod 2016;95:1–12.
[39] Kowal J, et al. Proteomic comparison defines novel markers to characterize heterogeneous populations of extracellular vesicle subtypes. *Proc Natl Acad Sci* U S A 2016;113:E968–77.
[40] Konoshenko MY, Lekchnov EA, Vlassov AV, Laktionov PP. Isolation of Extracellular Vesicles: General Methodologies and Latest Trends. BioMed Research International 2018;2018:1–27.
[41] Jung MK, Mun JY. Sample preparation and imaging of exosomes by transmission electron microscopy. Journal of Visualized Experiments 2018;2018:1–5.
[42] Chuo STY, Chien JCY, Lai CPK. Imaging extracellular vesicles: Current and emerging methods. Journal of Biomedical Science 2018;25:1–10.
[43] Yellon DM, Davidson SM. Exosomes nanoparticles involved in cardioprotection? Circ Res 2014;114:325–32.
[44] Webber J, Clayton A. How pure are your vesicles? J Extracell Vesicles 2013;2.
[45] Forteza-Genestra MA, et al. Purity Determines the Effect of Extracellular Vesicles Derived from Mesenchymal Stromal Cells. Cells 2020;9:1–15.
[46] Brennan K, et al. A comparison of methods for the isolation and separation of extracellular vesicles from protein and lipid particles in human serum. Sci Rep 2020;10:1–13.
[47] Heath N, et al. Rapid isolation and enrichment of extracellular vesicle preparations using anion exchange chromatography. Sci Rep 2018;8:1–12.
[48] Liangsupree T, Multia E, Riekkola ML. Modern isolation and separation techniques for extracellular vesicles. J Chromatogr A 2021;1636:1–17.
[49] Wang L, Bruce TF, Huang S, Marcus RK. Isolation and Quantitation of Exosomes Isolated from Human Plasma via Hydrophobic Interaction Chromatography Using a Polyester, Capillary-Channeled Polymer Fiber Phase. Anal Chim Acta 2019;1082:186–93.
[50] Yakubovich EI, Polischouk AG, Evtushenko VI. Principles and Problems of Exosome Isolation from Biological Fluids. Biochemistry (Moscow) Supplement Series A: Membrane and Cell Biology 2022;16:115–26.